*mathematics*

MDPI

*Article*

# Generalised S-System-Type Equation: Sensitivity of the Deterministic and Stochastic Models for Bone Mechanotransduction

**Julijana Simonović [1,*] and Thomas E. Woolley [2]**

[1] Faculty of Mechanical Engineering, University of Nis, 18000 Nis, Serbia
[2] School of Mathematics, Cardiff University, Senghennydd Road, Cardiff CF24 4AG, UK; woolleyt1@cardiff.ac.uk
* Correspondence: simonovicjulijana@gmail.com or julijana.simonovic@masfak.ni.ac.rs

**Abstract:** The formalism of a bone cell population model is generalised to be of the form of an S-System. This is a system of nonlinear coupled ordinary differential equations (ODEs), each with the same structure: the change in a variable is equal to a difference in the product of a power-law functions with a specific variable. The variables are the densities of a variety of biological populations involved in bone remodelling. They will be specified concretely in the cases of a specific periodically forced system to describe the osteocyte mechanotransduction activities. Previously, such models have only been deterministically simulated causing the populations to form a continuum. Thus, very little is known about how sensitive the model of mechanotransduction is to perturbations in parameters and noise. Here, we revisit this assumption using a Stochastic Simulation Algorithm (SSA), which allows us to directly simulate the discrete nature of the problem and encapsulate the noisy features of individual cell division and death. Critically, these stochastic features are able to cause unforeseen dynamics in the system, as well as completely change the viable parameter region, which produces biologically realistic results.

**Keywords:** mathematical model of osteocyte mechanobiology; external periodic excitation; mechanotransduction; bone remodelling; population model; autocrine/paracrine signalling

**Citation:** Simonovic, J.; Woolley, T.E. Generalised S-System-Type Equation: Sensitivity of the Deterministic and Stochastic Models for Bone Mechanotransduction. *Mathematics* **2021**, *9*, 2422. https://doi.org/10.3390/math9192422

Academic Editor: Theodore E. Simos

Received: 18 August 2021
Accepted: 26 September 2021
Published: 29 September 2021



## 1. Introduction

The architecture and quality of bone tissue in an adult organism predominantly depends on bone cellular organisation and communication processes that are highly driven by external mechanical loading. One major interest of mechanobiology is how physical forces and changes in the mechanical properties of cells and tissues contribute to development, cell differentiation, physiology, and disease. Critically, bone-adaptive mechanobiological processes are governed by multiple cellular populations, namely, osteoblasts, osteoclasts, and osteocytes, which all work in concert and capable of transducing mechanical strain signals into biochemical cues for osteogenesis [1,2]. The abundant presence of osteocytes (OcY) in bone lacunae makes them predominant, with 90–95% presence compared to all other bone cellular lineages. They are also the longest living bone cell. This high proportion of osteocytes is important, because not only have they recently been shown to be the most mechanosensitive bone cell type, but they have also been observed to direct osteogenesis in other bone cell types [3,4]. Thus, it has been suggested that osteocytes are able to combine these two properties and orchestrate adaptive bone remodelling that is dependent upon their mechanical sensitivity [5]. Unfortunately, direct, in vivo experimental observation of osteocytes has proven extremely challenging because they exist deep within the bone matrix. Thus, how osteocytes experience, sense, and transmit mechanical stimuli is an open question. Specifically, although we can quantify tissue-level

changes to mechanical loading, we currently have no connection between these macroscopic effects and the microscopic molecular mechanisms that give rise to these changes.

Here, we focus on bone remodelling, a cyclic process that is performed by groups of bone-resorbing osteoclasts (OCs) and bone-forming osteoblasts (OBs) that are combined together in "basic multi-cellular units" (BMUs). Essentially, these two cellular families must work together to ensure that neither too much nor too little bone is being created. If this balance of formation and resorption is not correctly regulated, bone disorders can form, such as bone cancer, osteoporosis, and Paget's disease. Since there are still many questions relating to how the large number of interconnected components (e.g., hormone, tumour cells, immune cell) signal to one another [3,5], mathematical models have been created to allow us to highlight what is known and hypothesise about what is consistent with the available data [6–10]. These mathematical models consist of ordinary differential equations and allow us to dynamically track cell numbers, components interrelations, and the bone volume over time. The idea is that once we are able to produce a simulated system that can be used to understand a homeostatic system, we would then be able to investigate the model and predict therapeutic strategies that could aid in cases where problems are seen [8].

The development and function of the BMUs depend as much on cellular communication processes as on the physical forces acting upon and transmitted by its constituent cells. However, a whole concept of how the cells and the mechanical signals interact, and how the local cellular and global loading processes are interrelated, is still a developing field of mechanobiology [1,11–14]. Modern imaginative and refined experimental strategies using genetics, imaging, quantitative (real-time) measurements and biophysical approaches, such as bone-on-chip devices or bioreactors, combined with mathematical modelling are necessary to understand the cellular and developmental processes of mechanosensitivity and adaptivity.

Bone tissue remodelling is a highly multiscale process, as such a single in vitro, or in silico, model would not be able to capture this entire complexity. Thus, we must focus on specific aspects of the bone remodelling process and ensure that our questions are specific enough that the model we use is able to accurately investigate them. Equally, parameterization of an established accompanying mathematical model is difficult, given its dependency on the accuracy and availability of data [9]. Critically, our models generate continuum trajectories of the evolving populations, whereas the current available data from in-vitro experiments provides only discrete time snapshots of a few measurable variables. However, having in mind the presence of noise, stochastic influence, and high sensitivity of these systems, the dynamics between certain points may differ from the one that is directly predicted by interpolations. For example, our analysis shows the presence of relatively large fluctuations over a short time span. Therefore, although models may match data at specific time points, due to numerical adjustment algorithms, models between these measurements may report behaviours not yet detected by biological experiments.

Equally, the ability to extrapolate our mathematical understanding must be considered. For example, in vitro experiments can last up to fourteen days in controlled conditions. However, the bone remodelling period can last up to 120 days, as suggested in [15], and mathematical models can give predictions on even longer time scales. However, although interpolation and extrapolation may be possible, we need to ensure that any results we generate through appropriate analytical procedures [16] are robust to the addition of new, more realistic features. Specifically, proposed key results in previous literature should not be sensitive to an increase in complexity of our mathematical model. As such, we seek to extend the current models of bone remodelling [6–9,15,17,18] to include stochastic features, which have been ignored until now.

Here, we use mathematical models to improve our current understanding of mechanobiology and its specific role in bone remodelling. Critically, whilst our model maintains those fundamental mechanisms highlighted in previous work [6–9,15,17], we include additional features of mechanosensitivity and, simultaneously, simulate these models under

the understanding that the populations are discrete-valued, rather than continua. Specifically, we include osteocytes mechanobiology, which, apart from the biochemical processes of osteocytes and their interactions with other bone remodelling cells, includes external periodic signal transduction and influences that represent a significant advance in the field.

The generalized form of an earlier stated cell population model consisting of a system of ordinary differential equations (ODEs) is presented together with a summarized explanation of all the parameters involved for the particular case of five ODEs. The extension of this system is presented in the form of additional periodic terms in the equation of OcY time changes, which extends the mathematical modelling of bone mechanobiology. Using a Stochastic Simulation Algorithm (SSA) to simulate the creation and degradation, which encapsulates the noisy features of individual cell division and death, we create statistically exact realizations of the system. The realizations are statistically exact in the sense that the simulated ensemble data converges to the distribution that solves the underlying stochastic problem. The SSAs are done by generating two random variables, one to define the time at which the next reaction occurs and one to specify the reaction that occurs. Critically, we use the Law of Mass Action to provide a correspondence between the deterministic rates of reaction (seen in the differential equations) and the probabilistic rates used in the SSA. Thus, we suppose that there are $N$ reactions involving $n$ species. The probability of a reaction firing is proportional to the product of the input populations. Intuitively, reactions with higher rates are more likely to occur. Following this stochastic formulation, we define a probability distribution for parameters of external excitation through fitting the model to data. These distributions allow us to investigate the sensitivity of the model formulation. Finally, the derivation and simulation of corresponding stochastic models allows us to question the utility of the deterministic simulations.

Our model is a time-dependent description of biological parameters and mechanical stimuli that influence bone remodelling by mechanotransduction of the received and sent signals by OcYs. Due to the microscopic/discrete view of the population, we are only interested in a small length scale where diffusion is irrelevant. It allows us to represent and explain as many parameters as are known from biological experimentation and to reveal their influence and importance. Furthermore, the stochastic analogue that we introduce shows that incorporated reception and transduction of signals changes the underlying dynamics of the cell communication processes.

Although we ignore spatial effects, there are researchers considering the wider view of bone remodelling [14,19], who include space–time displaced effects that are involved in the bone reconstruction process. These approaches, mainly based on an integro-differential system of diffusion–reaction equations, allows us to investigate the spatial aspects of the problem such as how far can mechanical signals travel? Moreover, how long do such signals take to travel these distances? Even though several possible simplifying assumptions have been proposed to give an answer to these questions [19], stochastic spatially extended systems need further investigation. Critically, extending diffusive movement to include stochastic effects is fairly simple [20] and is an avenue for later investigation.

## 2. Methods and Mathematical Models

The formalism of a cell population model can be generalised to be of the form of an S-System of $n$ equations [21], with $n$ corresponding to the number of included cellular lineages:

$$\frac{du_i}{dt} = \sum_{k=1}^{n} \alpha_k \prod_{j=1}^{n} u_j^{\gamma_{ijk}} - \beta_i u_i;\ i = 1, 2, \ldots, n, \quad (1)$$

This is a system of nonlinear ordinary differential equations (ODEs), each with the same structure: the change in a variable is equal to a difference of a product of power-law functions with a specific variable. The $u_i$ are the concentrations of a variety of biological

populations involved in bone remodelling (e.g., cell lineages, proteins, and other gene products). They will be specified concretely in the case of the specific system as considered in Table 1. The $\alpha_i$ are the creation rates that express how each population differentiates and/or proliferates. The $\beta_i$ represent the degradation rate of each signalling population. The $\gamma_{ij}$ represent the nonlinearities present in the population interactions. If we include OcY, OB, OC, and pre-osteoblastic (pOB) lineages of cells together with a bone mass equation, it will be a system of five equations ($n = 5$). System (1) is a homogeneous system of coupled ordinary nonlinear differential equations that is more specifically described in Table 1, where the coupling means that the variables appear in each other's equations. The table also contains explanations of all the parameters. In one cycle of targeted remodelling, the number of activator cells inside one basic bone multicellular unit (BMU), both resorbing and forming, is bounded above by approximately 10 OCs and up to 300 OBs. Critically, the continuum formulation of system (1) suggests that non-integer cellular population values can be obtained. Normally, such ODEs represent concentrations and densities, which themselves represent many individuals. In such cases, non-integer values are simply seen as approximations to the true underlying values because the resulting errors are small. However, in our case of small population numbers, such non-integer results are no longer valid approximations to the discrete values the biological populations can take.

**Table 1.** Mathematical model (1) with the description of all parameters, taken from [9] and also very similar to [6].

| Equation Interpretation | Variable and Parameter Explanation |
|---|---|
| $\frac{dS}{dt} = \underbrace{\alpha_1}_{OB\ embbeding\ rate} B^{\gamma_{31}} \left(1 - \frac{S}{K_s}\right)_+ - \underbrace{\delta S}_{apoptosis}$ (2)<br>change in osteocyte = increase due to embedded osteoblasts − apoptosis<br>Sclerostin is produced by osteocytes and inhibits the Wnt/$\beta$-catenin pathway. Wnt is known to promote osteoblastic proliferation and differentiation. We incorporate the effects of sclerostin and the Wnt/$\beta$-catenin pathway into the mathematical model through a term of the form $\left(1 - \frac{S}{K_s}\right)_+$, where $(x)_+ = max(x, 0)$ and $K_s$ is a parameter that describes the relation between osteocyte apoptosis and decrease in sclerostin inhibition. The idea is that, for a threshold level $K_s$ of osteocytes, there is sufficient sclerostin production to inhibit local Wnt signaling. When osteocytes die, the sclerostin level decreases. This releases osteoblast precursor cells from Wnt inhibition, thereby initiating a cycle of targeted bone remodelling. | $S$ number of OcYs and<br>$B$ number of OB at a given time $t$<br>OcYs are mature OBs that become embedded in extracellular matrix at a given rate $\alpha_1$<br>$\gamma_{31}$ effectiveness of OB autocrine signalling<br>$K_s$ critical value of OcY population<br>$\gamma_{31}$ effectiveness of OB autocrine signalling<br>$\delta$ rate of OcY apoptosis,<br>$\delta = 0$ over the time scale of single event of targeted remodelling; the most significant influence on osteocyte apoptosis is the initial biomechanical action that begins remodelling (initial condition). |
| $\frac{dB_P}{dt} = \underbrace{\underbrace{\alpha_2 S^{\gamma_{21}} \left(1 - \frac{S}{K_s}\right)_+^{\gamma_{22}}}_{paracrine\ promotion} + \underbrace{\alpha_3 B_P^{\gamma_{32}} \left(1 - \frac{S}{K_s}\right)_+}_{autocrine\ promotion}}_{pre-osteoblast\ differentiation\ and\ proliferation} - \underbrace{\beta_1 B_P^{\varphi_{12}} C^{\varphi_{14}}}_{\substack{pre-osteoblast\ differentiation \\ to\ mature\ osteoblast}} - \underbrace{\delta B_P}_{apoptosis}$ (3)<br>change in pre-osteoblast = increase due to differentiation of stromal cells (released from sclerostin or exposure to growth factors) + proliferation of pre-osteoblasts (autocrine signalling of Wnt and growth factor) − differentiation to osteoblasts (growth factor) − apoptosis | $B_P$ number of pre-osteoblast (pOB) at a given time $t$<br>$\alpha_2$ differentiation rate of pre-osteoblast precursors from the large pool of stem cells in response to signalling molecules produced by OcY<br>$\alpha_3$ pre-osteoblast proliferation rate<br>$\beta_1$ differentiation rate of pre-osteoblasts to become mature OBs<br>$\gamma_{21}$ effectiveness of OcY paracrine signalling of pre-osteoblasts<br>$\gamma_{22}$ effectiveness of sclerostin regulation of osteoblastogenesis |

| | |
|---|---|
| | $\gamma_{32}$ effectiveness of pre-osteoblast autocrine signalling |
| | $\varphi_{12}$ effectiveness of pre-osteoblast autocrine signalling of osteoblasts |
| | $\varphi_{14}$ effectiveness of OC paracrine signalling of pre-osteoblasts (for example the effect of TGF-$\beta$ on pre-osteoblasts) |
| | $\delta$ rate of pre-osteoblasts apoptosis |
| $\frac{dB}{dt} = \underbrace{\beta_1 B_P^{\varphi_{12}} C^{\varphi_{14}}}_{\substack{pre-osteoblast\ differentiated \\ to\ mature\ osteoblast}} - \underbrace{\beta_2 B^{\varphi_{23}}}_{apoptosis} - \underbrace{\alpha_1 B^{\gamma_{31}} \left(1 - \frac{S}{K_s}\right)_+}_{embedding\ as\ osteocytes}$ (4) | $B$ number of OB at a given time $t$ |
| | $\varphi_{23}$ effectiveness of OB autocrine signalling for apoptosis |
| change in osteoblast = increase due to differentiation of pre-osteoblast (growth factors) $-$ apoptosis $-$ embedding as osteocytes | $\beta_2$ rate of OBs apoptosis |
| $\frac{dC}{dt} = \underbrace{\alpha_4 S^{\gamma_{41}} B_P^{\gamma_{42}} (\varepsilon + B)^{\gamma_{43}} \left(1 - \frac{S}{K_s}\right)_+^{\gamma_{44}}}_{paracrine\ promotion} - \underbrace{\beta_3 C^{\varphi_{34}}}_{apoptosis}$ (5) | $C$ number of OCs at a given time $t$ |
| | $\gamma_{41}$ effectiveness of OcY paracrine signalling of OCs derived by RANKL |
| change in osteoclast = increase due to differentiation of pre-osteoclast (due to RANKL and limited by OPG) $-$ apoptosis. | $\gamma_{42}$ effectiveness of pre-osteoblast paracrine signalling of osteoclasts |
| The term $(\varepsilon + B)^{\gamma_{43}}$ represents the effect of OPG acting as a decoy receptor for RANKL. In models of [6] without pre-osteoblasts ($B_P = 0$), the parameter $\gamma_{43}$ takes on a negative value, and since for that case $B$ has 0 as steady state value it is necessary to add a sufficiently small number $\varepsilon$ to avoid dividing by zero. This represents the factor of production when $B = 0$. | $\gamma_{43}$ effectiveness of OB paracrine signalling of OCs |
| | $\gamma_{44}$ effectiveness of sclerostin regulation of osteoclastogenesis |
| | $\beta_3$ rate of OC cell death |
| | $\varphi_{34}$ effectiveness of OC autocrine signalling for apoptosis |
| $\varepsilon(x) = \frac{1+\mathrm{sgn}(x)}{2} = \begin{cases} 0, & if\ x<0 \\ 1/2, & if\ x=0 \\ 1, & if\ x>0 \end{cases}$ The Heaviside function is a non-continuous function whose value is zero for a negative input and one for a positive input. This explanation is from [9], however we did not use this function in our stochastic system. | $\varepsilon$ Heaviside function |
| | $\alpha_4$ differentiation rate of OCs precursor |
| $\frac{dz}{dt} = k_1 v_1 - k_2 v_2\ for$ $v_i = \begin{cases} u_i - \overline{u_i}, if\ u_i > \overline{u_i} \\ 0, if\ u_i \le \overline{u_i} \end{cases}$; $u_1 = B$; $u_2 = C$; $i = 1,2$ (6) | $z$ changes in bone mass (the total new bone content) over time relative to the initial value of 100% |
| Changes in bone mass = increase due to activity of osteoblasts $-$ activity of osteoclasts | $k_1$ normalized activities of bone formation and $k_2$ normalized activities of bone resorption |

Critically, the problem stems from the direct use of differential equations that assume a modelled population is large enough for a continuum hypothesis to approximately hold. This hypothesis is obviously invalid at such small population sizes. Thus, for such low numbers of cells, it is more correct to produce a discrete interaction model. Specifically, we use a stochastic framework to simulate the creation and degradation, which encapsulates the noisy features of individual cell division and death [22–26].

We could model the system using a chemical master equation (CME), which provides an exact description of the evolution of the probabilities of the active species being in a certain state. By deriving the CME, we ignore an individual's specific positions and velocity as the system is reduced to specifying only the populations and interactions between them. Namely, we assume that space is not an issue we need to consider. As such, the model explicitly assumes that any cellular population is within contact range of any other; thus, interactions are rate limited, not diffusion limited. Although the general CME can be derived, in most cases it has a high dimension and is nonlinear; thus, exact solutions

exist only in rare cases. However, it can be solved in the sense of using Stochastic Simulation Algorithms (SSAs) to create statistically exact realizations of the system, where averaging over many simulations is equivalent to solving the CME. Here, the solutions are "statistically exact" in the sense that the ensemble distribution, produced through a very large number of simulations, converges to a probability distribution that would be an exact solution of the stochastic system.

The basic premise of an SSA is to sample paths from a derived probability distribution. This is done by generating two random variables, one to define the time at which the next reaction occurs and one to specify the reaction that occurs. Critically, we use the Law of Mass Action to provide a correspondence between the deterministic rates of reaction (as expressed by the differential equations) and the probabilistic rates used in the SSA. Thus, we suppose that there are $N$ reactions involving $n$ species. The probability of a reaction firing is proportional to the product of the sizes of the input populations. We consider here the input populations of only those involved in the specific reaction. Intuitively, reactions with higher rates are more likely to occur [26]. The reaction probabilities are known as propensity functions, $a_j(u_1, u_2, \ldots u_n), j = 1, \ldots, N$.

To calculate which reaction is going to fire individual reaction rates are normalized by the total of all reaction rates, $a_0 = \sum_{j=1}^{N} a_j$, which converts the rate of each reaction into a probability; thus, the cumulative sum of all reaction probabilities is 1. A uniformly distributed random number, $U$, is chosen from the interval [0, 1] and this number is compared to the cumulative sum of the propensity functions. The reaction $J$ $(1 \le J \le N)$ that is chosen to fire is defined to be the one that causes the cumulative sum of the propensity functions to breach the random number (see Figure 1), in the following manner:

$$\frac{1}{a_0}\sum_{j=1}^{J-1} a_j < U \le \frac{1}{a_0}\sum_{j=1}^{J} a_j, \tag{7}$$

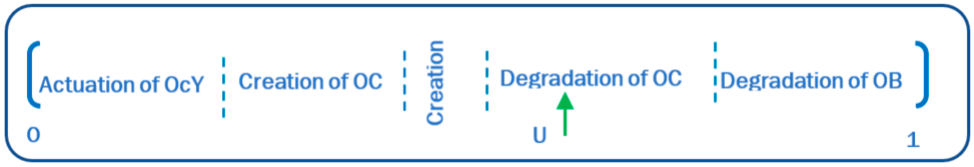


**Figure 1.** Schematic diagram of how the next action in a stochastic simulation is calculated, a visual representation of Equation (7). The rates of all actions (creation and degradation of OC and OB, and/or OcY embedding) are calculated using the Law of Mass Action. These rates are then converted to probabilities by dividing each one by their sum. While a uniformly distributed random number $U$ is chosen between zero and one it will allow the next action to occur, namely, "Degradation of OC".

A similar manipulation, involving sampling from an appropriate Poisson distribution that is created from the reaction rates, provides a probability distribution when this next reaction occurs [23,25–29], namely, if we are currently at time $t$ then the next reaction fires at $t + \Delta t$, where

$$\Delta t = \frac{1}{a_0}\ln\left(\frac{1}{r}\right),$$

and $r$ is a random number sampled from a uniform distribution on the interval (0,1). The populations are then updated in accordance with the action that has occurred, the system time is increased by the random time step, $\Delta t$ [23,26–29]. This process is then repeated until the system time has reached a specified limit.

From system (1) we can extract the stochiometric creation and degradation relations, and present their probabilistic analogues:

$$\gamma_{i1}u_1 + \gamma_{i2}u_2 + \cdots + \gamma_{in}u_n \xrightarrow{\alpha_i} \gamma_{i1}u_1 + \gamma_{i2}u_2 + \cdots + (\gamma_{ii}+1)u_i + \cdots + \gamma_{in}u_n, \tag{8a}$$

$$u_i \xrightarrow{\beta_i} \emptyset, i = 1, 2, \ldots, n, \tag{8b}$$

where now we are considering the $u_i$ to be representatives of a population of discrete individuals, rather than a continuous quantity. Further, the $\emptyset$ in Equation (8b) represents degradation to a population that is not being considered, i.e., the population is being eliminated. Note that the transition arrows used in Equations (8a) and (8b) do not represent limits of functions. Rather, the arrows represent a change from one biological species to another [29].

We use Equations (8a) and (8b) as examples of how to generate propensity functions. Namely, the creation and degradation propensities would, respectively, be

$$a_i^c = \alpha_i \prod_{j=1}^{n} u_j(u_j - 1) \ldots (u_j - \gamma_{ij} + 1) \text{ and } a_i^d = \beta u_i;\ i, j = 1, 2, \ldots, n. \tag{9}$$

In the next section, we present the results of stochastic simulations to demonstrate that the model captures the required autocrine, paracrine, and synergistic characteristics of bone remodelling.

The $\gamma_{ij}$ exponents are defined in terms of effectiveness in Table 1. However, in case that a number of interacting cells is effective in producing a new cell of some type, this is expressed as a factor, not as an exponent. Exponents usually model the number of interactions (or meetings or collisions etc.) involved in a transition. So, the $\gamma_{ij}$'s model the number of cells that (are required to) interact in order to produce a new cell, representing in that way the effectiveness of the auto/paracrine signalling (interactions).

If we assume there is no external stimuli, then system (1) should eventually tend to a stable steady state. Namely, the osteoclast and osteoblast populations are approximately constant over time and the populations stay close to these steady states after any subsequent small perturbations to the population sizes. Simultaneously, we want the system to be sensitive to external influences. Thus, we would expect the parameterisation of the system to cause it to lie near a bifurcation point, such that under standard conditions the system would replicate the desired stability of the steady states, but under perturbed parameters this stability to small perturbations would be lost [18]. However, operating near to a bifurcation does pose risks that unexpected stimuli will cause the system's steady states to tend in pathological directions. Thus, in such a biological system there has to be a balance of sensitivity, robustness, and state buffering.

Since it has been experimentally shown [30] that system (1) operates close to a region of instability, it is reasonable to perform stochastic simulations of system (7), not only because the dynamics are more accurate but also highlight how the noise can generate fundamentally different dynamic behaviours.

Although parameter values exist in the literature, they are approximate and are proposed to simplify and justify the model. Further, in all the literature, it is assumed that the $\gamma_{ij}$ parameters are constant. However, in real bone remodeling processes, the $\gamma_{ij}$ parameters may depend on time and other factors. Unfortunately, these parameters cannot be directly measured and must be estimated. Thus, although initially we consider constant parameters (which simplifies the mathematical treatment and gives a high level of approximation but is useful as a benchmark for model validation), we later extend the equation's constant parameters to include an oscillatory temporal dependence. The idea of this extension is based on the in vitro experiment of loaded OcYs cell cultures. Osteocytes express RANKL (the ligand of receptor activator of nuclear factor κβ protein (RANK)) and a macrophage-colony stimulating factor (M-CSF) to promote, and osteoprotegerin (OPG) and nitric oxide (NO) to inhibit, OC formation and activity. OcYs also regulate bone formation via the secretion of modulators of the Wnt signalling pathway. Prostaglandin $E_2$ (PGE2), NO, and adenosine triphosphate (ATP) act to activate wingless and Int-1 (Wnt) signalling, whereas sclerostin, DKK1 (negative regulators of the Wnt/β-catenin pathway

such as Dick-Wnt/β–catenin Kopf 1-related protein 1 (DKK1)), and SFRP1 (secreted frizzled-related protein 1, which is a competitive antagonist of Wnt ligand binding) all inhibit Wnt signalling and subsequent osteoblast activity [6,12,13]. There is strong evidence from in vitro experiments with single cells exposed to fluid shear flow and simultaneous monitoring of $Ca2^{+}$ [13] that mechanical stimulation of osteocytes activates $Ca2^{+}$-dependent contractions and enhances the production and release of extracellular vesicles containing these bone regulatory proteins, suggesting a critical role for $Ca2^{+}$-mediated OcYs signalling in bone adaptation. Furthermore, it was reported that the frequencies of the load-induced $Ca2^{+}$ transients and cell actin contractions have not been found significantly different, suggesting their coordination in response to mechanical load.

Based on these recent findings, we introduce the modification of the model by editing the power term $\gamma_{31}$ to time-dependent oscillatory function $\gamma_{31}(1+\sin(\theta t))$, which represents a transduced signal of OcY, and inserting the mechanical periodic excitation $A(1-\cos(\theta t))$ to the responding OcYs into the following form:

$$\frac{dS}{dt} = \underbrace{\alpha_1}_{OB\ embbeding\ rate} B^{\gamma_{31}(1+sin\,\theta t)}\left(1-\frac{S}{K_s}\right)_+ + A(1-cos\,\theta\, t), \tag{10}$$

Critically, the parameter values, which were derived using the deterministic equations, defined in Table 2, often provide cellular populations that breach the expected upper population limits in the stochastic simulations (that is 300 cells of OBs) (see the yellow lines in Figures 2A–C and 3A). To counter this, we alter the equations in Table 1, such that the $B$ terms on the right-hand side of all equations are adapted to become $2B$, which usually (stochastically speaking) reduces the populations down to a biologically expected size. Equivalent variations to the parameter values, rather than the kinetics, are equally possible, namely, the factor of 2 would be combined with other parameters, leading to slightly altered values. Here, however, we move forward with the simpler version of altering the kinetics. Critically, the rescaling of $B$ to $2B$ comes from an anthropic argument of this is what is required to fit the data (or at least the order of magnitude). Thus, it becomes a prediction of the model.

We should note that we are note really interested in the role of specific parameter values; rather, we are considering the influence of noise on models. The subject of our next manuscript will be following this stochastic formulation as we will be able to then define a probability distribution for each parameter value through fitting the model to data. There are many ways that such distributions can be extracted [31], but our preferred method would be to use a Bayesian approach, which supplies the confidence distribution of a parameter dependent on the evidence we have [32]. These distributions will then allow us to investigate the sensitivity of the model formulation. However, such work is outside of our current scope.

The frequencies, $\theta$, of the received and transduced signal are the same in both functions but with some delay, represented as the phase shifting of $\pi/2$ or $\pi$ in the following simulations.

**Table 2.** Parameter values for the system in Table 1. Unless otherwise stated, these values are fixed across all simulations and are taken from [9]. The unit of each parameter is taken to ensure that the output rate is on the scale of cells/day.

| **Parameter Name** | $\boldsymbol{\alpha_1}$ | $\boldsymbol{\alpha_2, \alpha_3, \alpha_4, \beta_1, \beta_2, \beta_3, \delta}$ | $\boldsymbol{K_s}$ | $\boldsymbol{k_1}$ | $\boldsymbol{k_2}$ | $\boldsymbol{\gamma_{31}, \gamma_{21}, \gamma_{22}, \gamma_{32}, \gamma_{41}, \gamma_{42}, \gamma_{44}}$ | $\boldsymbol{\gamma_{43}}$ | $\boldsymbol{\varphi_{12}, \varphi_{14}, \varphi_{23}, \varphi_{34}}$ |
|---|---|---|---|---|---|---|---|---|
| Parameter value | 0.5 | 0.1 | 200 | 0.7 | 0.015445 | 1 | −1 | 1 |

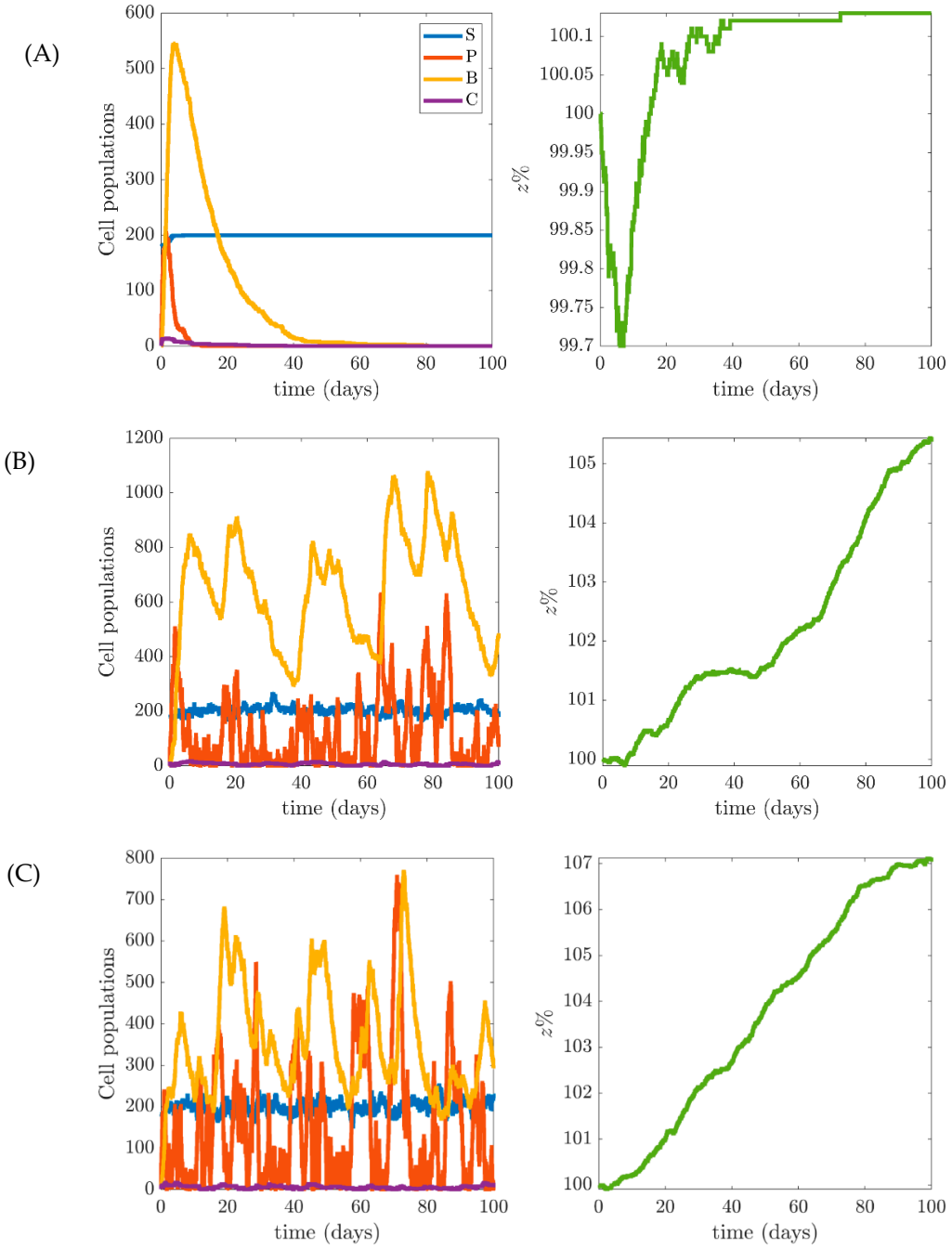


**Figure 2.** (**A**) The number of osteocytes (OcY) is restricted to a maximum of 200 cells. (**B**) The number of OcY is unrestricted and has small oscillations around a number of 200 but the number of OB has unexpected increases up to 1200 cells, which is unrealistic during one cycle of bone remodelling. (**C**) The same as (**B**), but the equations have been altered to ensure that OB does not spike beyond 600 such that the $B$ terms on the right-hand side of all equations are adapted to become $2B$. All diagrams correspond to the same system of equations without external signalling. The same legend shown in (**A**) left corresponds to all left diagrams, where S (blue line) represents OcYs dynamics, P (red line) represents pOBs dynamics, B (yellow) represents OBs dynamics, and C (purple line) represents OCs dynamics.

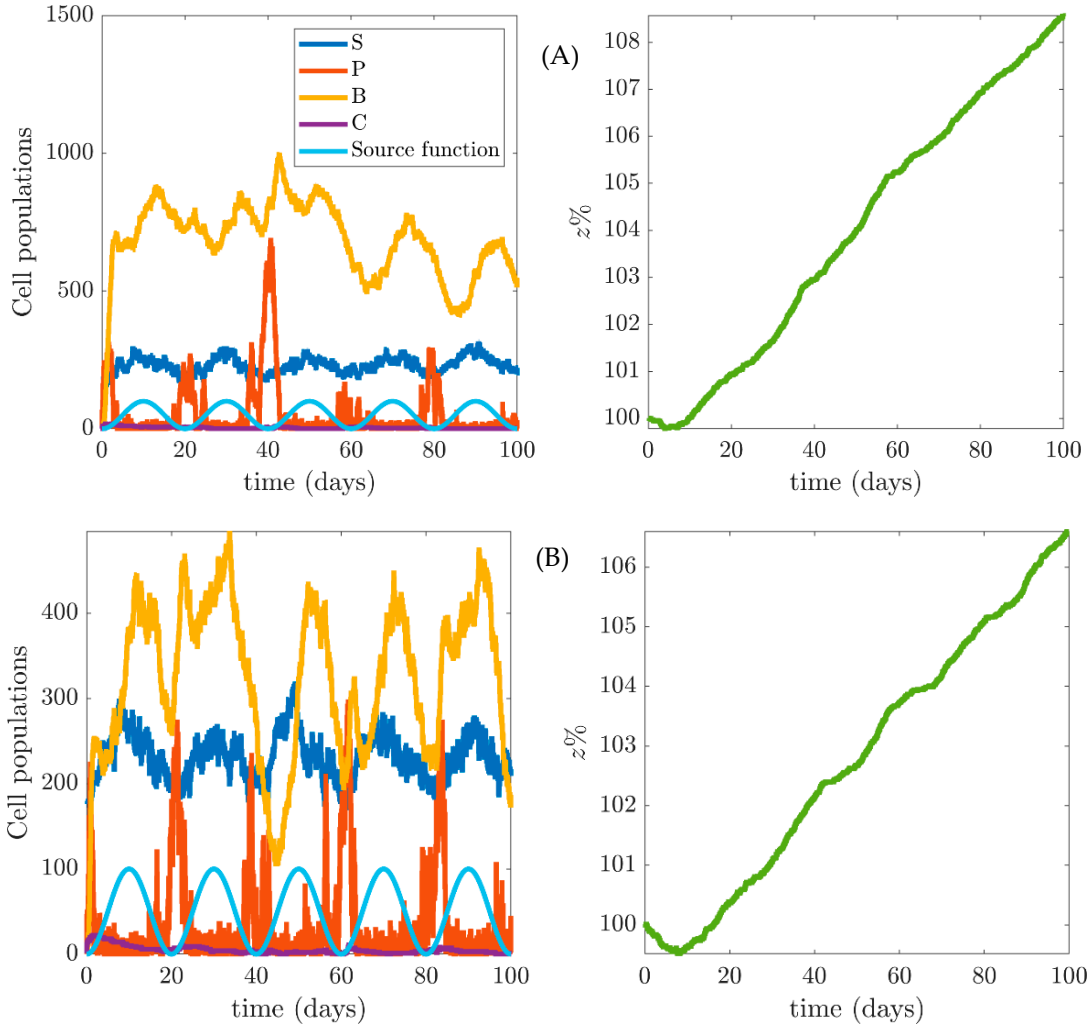


**Figure 3.** External excitation disturbed the source of OcY numbers describing the number of affected responding OcY in the BMU. (**A**) External periodic source (light blue line) that affects number of active OcY (S line). (**B**) The equations have been altered to ensure that OB does not spike beyond 600, such that the $B$ terms on the right-hand side of all equations are adapted to become $2B$. The same legend shown at (**A**) left corresponds to the left diagram at (**B**), where S (blue line) represents OcYs dynamics, P (red line) represents pOBs dynamics, B (yellow) represents OBs dynamics, C (purple line) represents OCs dynamics, and Source function (pale blue line) corresponds to the external signal that the responding OcYs receive.

## 3. Results

The numerical calculation in deterministic system (1), i.e., (2)–(6), and the SSA of (7) was performed firstly with the system of parameter values given in Table 2. These particular values were chosen as they put the system in an "excitable state", namely, the system undergoes a large transient jump in population, before tending to the steady state values: $OB_{ss} = (B_{ss}) = OC_{ss} = (C_{ss}) = pOB_{ss} = (B_{Pss}) = 1, OcY_{ss} = S_{ss} = K_s = 180$ after approximately one hundred days. Using the algebraic computation software package, Maple [33], there are no other real steady states within the parameter region of interest. Since there are no interesting bifurcations near our point of interest, suggested by biological events, we do not include a parameter sweep analysis. However, a more global investigation of theoretical bifurcations is going to be investigated in future work. We got the same results with both the deterministic and stochastic calculations, Figure 2A, as it was exactly illustrated in [9]. Figure 2A shows the dynamics of bone volume (green line, z% in time (days)) during a single event of targeted bone remodelling. Starting with $z_{ss}$ = 100%, we notice that there is first a resorption phase (decrease in $z_{ss}$) due to an increase in the osteoclast cell numbers; in turn, this leads to a decrease in bone volume. The brief decrease phase is

followed by a bone formation phase because of increases in osteoblast cell number, so that we notice increase of total bone content up to 100.1% (see Figure 2A). The bone turnover is completely balanced if the amount of new bone formed equals the amount resorbed and z reaches 100%.

Mathematically, this corresponds to a steady-state value of bone mass. The steady-state value for bone volume, denoted $z_{ss^{ss}}$, depends significantly on the parameter values as it was claimed and shown in [9]. For instance, if the parameter values are such that there is an imbalance of OBs and OCs, in favour of OBs, then there will be over remodelling. Since this particular choice of values is more intuitive to describe the biological model of bone remodelling and far from real experimental readouts, we continue with the same model and in silico experiments but choosing different conditions, which better describe the same biological event. We introduce OcY mechanosensitivity features and find that they also considerably influence the dynamic of bone turnover. For instance, we ignore the positivity restriction of the $(1 - S/K_s)_+$ term, where $K_s$ is the osteocyte carrying capacity. The idea in [9] was that there exists a threshold level, $K_s$, of osteocytes, such that, at this point, there is sufficient sclerostin production to inhibit local Wnt signalling. When osteocytes die, due to the micro damage, the sclerostin level decreases [3,5]. Hence, OcY apoptosis can be a trigger for the next cycle to happen, as it was originally assumed in [9]. Specifically, in Figure 2B, the simulations eventually stop when $S = K_s$, because the term $(1 - S/K_s)_+$ in Equation (2) evaluates to zero and all dynamics stop, which is highly artificial. However, going forward, we simply consider the production rate of $S$ proportional to $(1 - S/K_s)$, whether positive or negative. This means that the number of OcY is unrestricted and the simulations are observed to have small oscillations around $K_s = 200$ cells per remodeling cycle (blue line on diagrams of Figure 2B,C).

Basically, this means that we assume there are a certain number of OcY ready to receive and send external signals and to open cell signalling channels in response to loading [4,11,12]. Similarly, we showed that the total bone content, in general, can also be controlled by considering the behaviour of OcYs mechanosensitivity (for instance, green line rapidly increases in Figure 2B,C).

We extended our investigations and considered the modification of Equation (2) in the form (10), i.e., by introducing OcYs reception and transduction of the external periodic signal. We explored firstly the independent influence of the additional terms:

(1) The intensity A in Equation (10) that represents an external activator signal that the responding OcY receives (Figure 3A,B);

(2) The periodic signalling that OcY send/receive and transduce from/to OB (Figure 4A,B).

An external source applied to OcY, the first case, introduced almost regular oscillatory behaviour of the OcY (S, blue line; Figure 3A,B) and OB (B, yellow line; Figure 3A,B), which is approximately in synchrony with the external signal (light blue line); however the bone content represents over remodelling since it constantly increases beyond 100%. The oscillatory changes in signalling parameter $\gamma_{31}(1 + sin\,\theta\, t)$, in the second case, cause the modulation of the OcY signalling with increased amplification (amplitude boosts) that corresponds to the maximal amplitude of the signalling changes (Figure 4).

Both additions of oscillatory phenomena give an increase of the total new bone content $z$ (green line on all diagrams), but in the first case, Figure 3, the increase is quite rapid and biologically inexplicable. More realistic and acceptable is bone content increase in the second case (Figure 4A,B), but in this case the behaviour of OBs (yellow line) and preosteoblasts pOBs (red line) are unpredictable and unexpected. Furthermore, the bone mass has a resorption phase (z% below 100%) of almost 70 days, which is not observed in the case of biological experiments, where the resorption phase lasts for 20 days.

The aforementioned oscillations happen together in the real event of receiving, transducing, and sending signals, so we apply both signals at the same time (Figures 5–7). The controlling parameter is the delay between receiving and transducing signals by the OcY

so that Figure 5 corresponds to maximal delay (a phase difference of $\pi$), such that when the external receiving signal is maximal there is no transduced signal and vice versa.

The simulation shown in Figure 6 is without a phase difference, the case when both signals are simultaneous; Figure 7 represents the case with a small delay (a phase difference of $\pi/2$) in the transduced signal, which is closer to real situation measured in the in vitro, single-cell experiments [13]. In any of these three cases, the behaviour changes of OcY are amplified periodically and followed with almost regular and synchronous changes in OB behaviour; however, the total bone content still permanently increases. These changes prove that signals sent to and from OcY enhance total bone mass, but still the engaged number of present active OB is considerably large, above 400, which cannot be taken as correct as we restricted our model to the size of the population active inside one BMU.

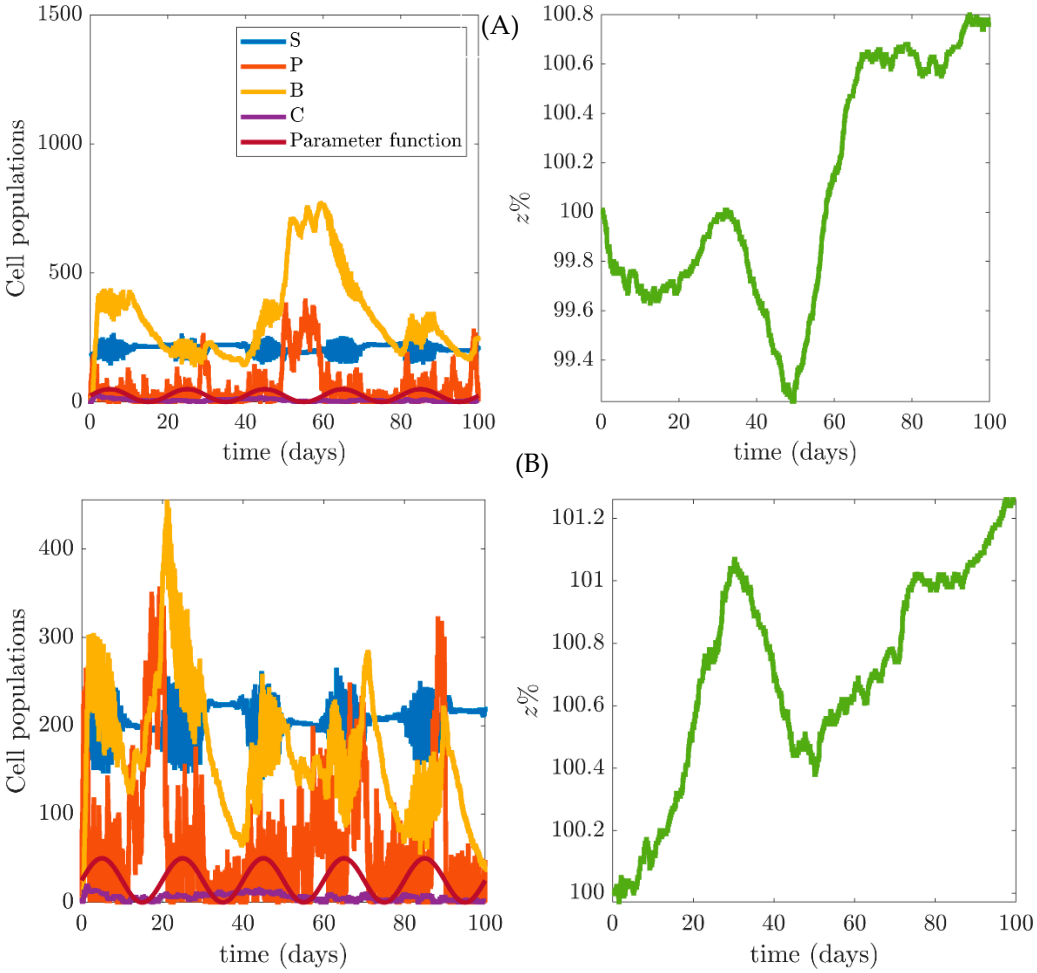


**Figure 4.** Oscillations in the external excitation effectiveness of OB autocrine signalling. (**A**) The maroon-coloured line illustrates the signalling parameter changes with magnitude $\gamma_{31}$ and causes synchronized boosts (amplitude modulated signal) in the OcY numbers (S line). (**B**) The equations have been altered to ensure that OB does not spike beyond 600 such that the $B$ terms on the right-hand side of all equations are adapted to become $2B$. The same legend shown in (**A**) left corresponds to the left diagram at (**B**), where S (blue line) represents OcYs dynamics, P (red line) represents pOBs dynamics, B (yellow) represents OBs dynamics, C (purple line) represents OCs dynamics, and Parameter function (Bordeaux line) corresponds to the signal that OcYs send to OB.

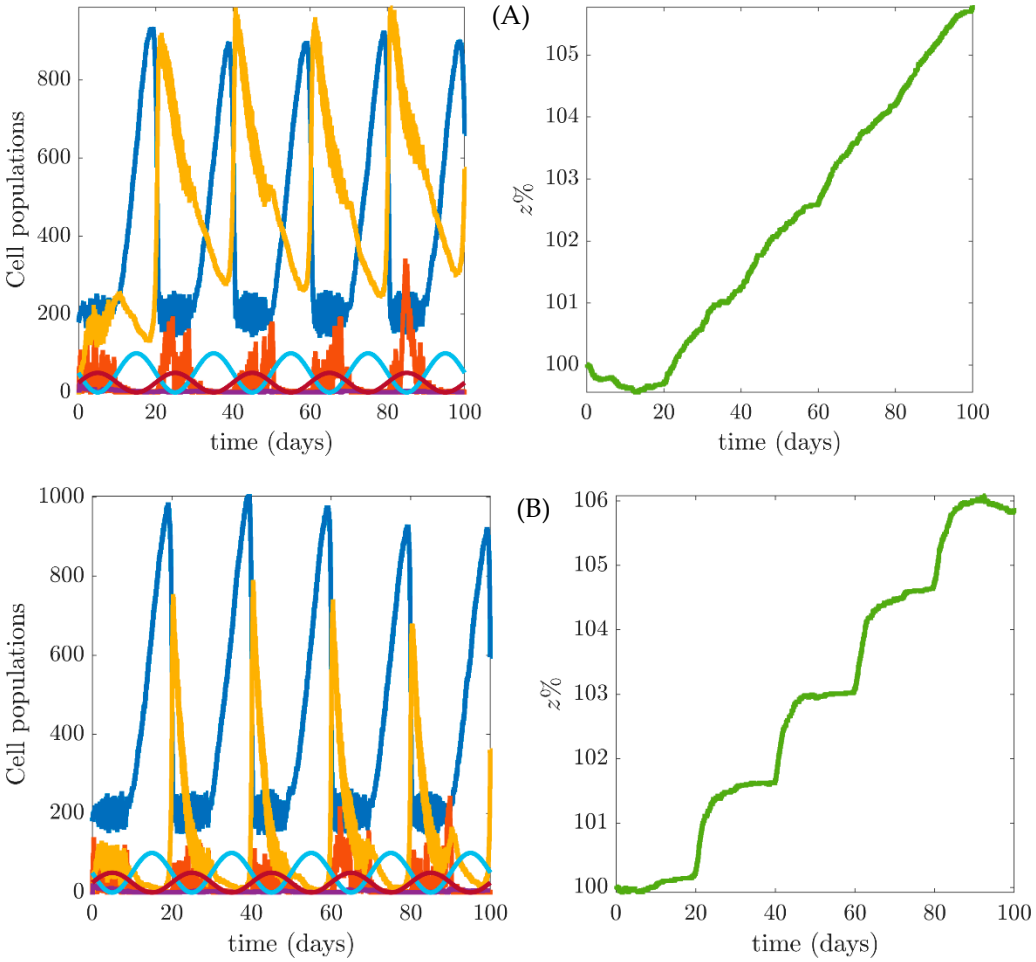


**Figure 5.** External excitation to both the parameter and the source. (**A**) External periodic source (light blue line) and parameter changes of magnitude $\gamma_{31}$ (dark red line) with phase difference $\pi$. (**B**) The equations have been altered to ensure that OB does not spike beyond 600, such that the $B$ terms on the right-hand side of all equations are adapted to become $2B$. The same legends from Figures 3 and 4A are applicable to these left diagrams.

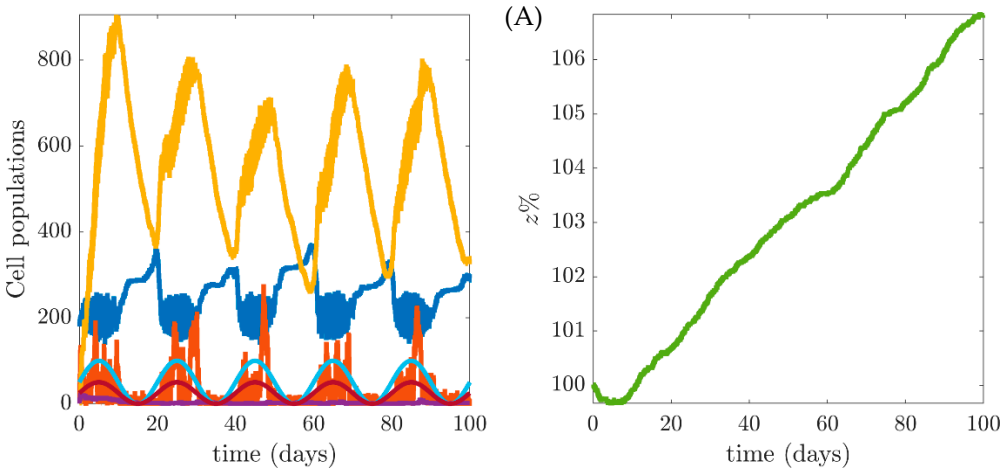

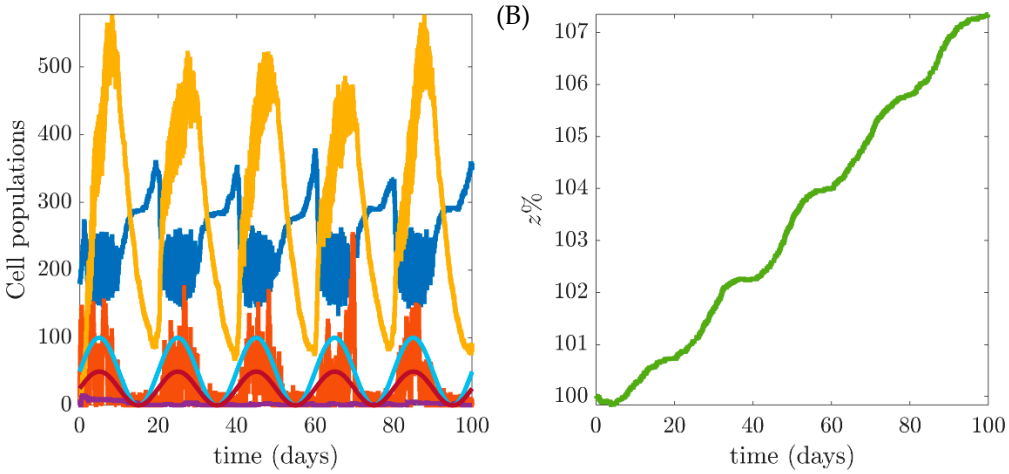


**Figure 6.** External excitation disturbed both to the parameter and to the source. (**A**) External periodic source light blue line and parameter $\gamma_{31}$ dark red line with phase difference 0. (**B**) The equations have been altered to ensure that OB does not spike beyond 600, such that the $B$ terms on the right-hand side of all equations are adapted to become $2B$. The same legends from Figures 3 and 4A are applicable to these left diagrams.

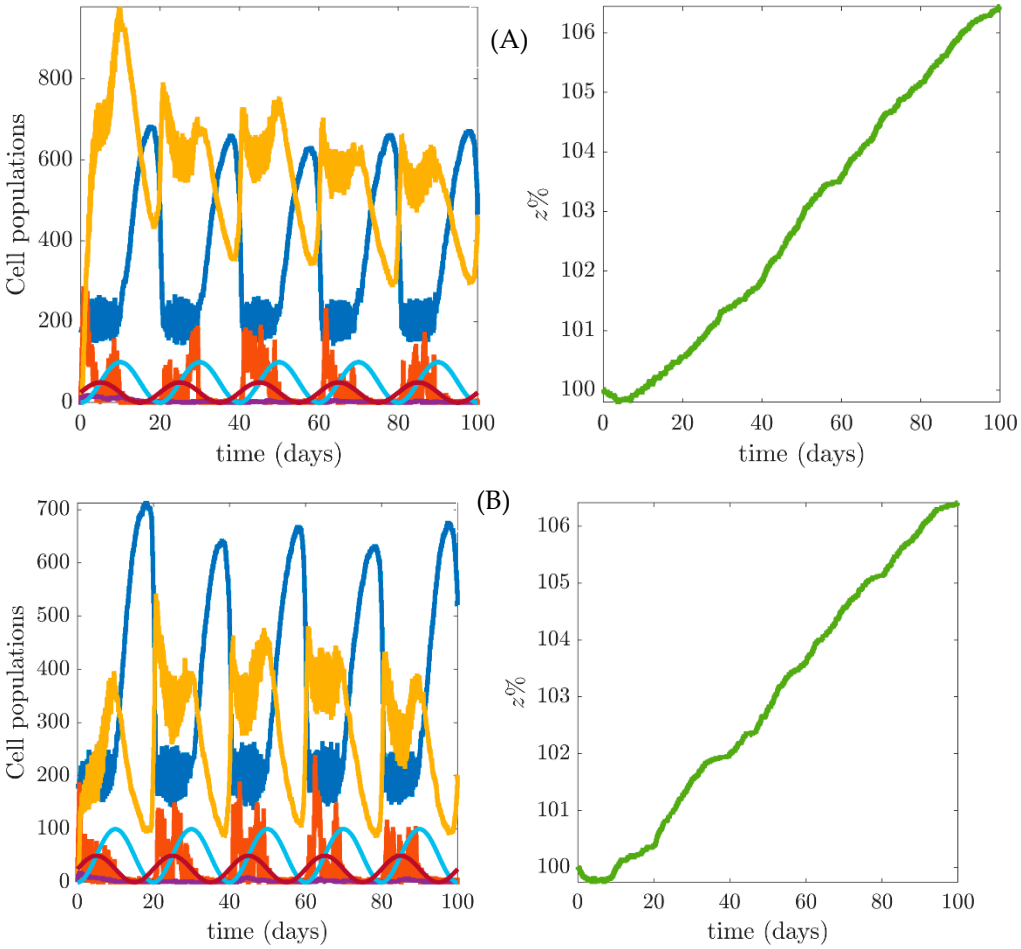


**Figure 7.** External excitation to both the parameter and to the source. (**A**) External periodic source light blue line and parameter $\gamma_{31}$ dark red line with phase difference $\pi/2$. (**B**) The equations have been altered to ensure that OB does not spike beyond 600, such that the $B$ terms on the right-hand side of all equations are adapted to become $2B$.

Further, numerical experiments in Figure 8 demonstrate that we could control the number of presented active cells by changing only the strength of the received signal.

Changes from $A = 50$, the value used for all simulations presented in Figures 2–7, to $A = 10$, the simulation presented at Figure 8, allow us to control the number of involved OB cells. Specifically, the value of OB cells density is around 200 per day in the biological model of a single, targeted bone remodelling event; this is the exact value around which OBs densities oscillates in Figure 8. Furthermore, to control the value of total bone content changes, we can count on small changes in the normalized activities of the bone resorption parameter $k_2$. If the green line goes beyond its stationary value, $z_{ss} = 100$, we refer to it as "over formation", which is when the new bone content exceeds the amount of resorbed old bone. This was the case in all in silico experiments presented in Figures 2–7. The green line goes beyond $z_{ss} = 100$, except in the specific case when we changed the normalized activities of bone resorption parameter $k_2$ in the system. The value was changed only a little, from $k_2 = 0.015445$, taken from [9]. to $k_2 = 0.014$.

These specific values of the parameters represent the situation of greater activity of the OC at the starting stage of the bone formation process (purple line Figure 8C), followed with the activity of the OB (yellow line), which illustrates a period of decline of $z$ below 100% for about 50 days and after bone mass grows above 100%, which represents the preferable influence of the appropriate transduction of an external periodic signal. These results link us to an expected behaviour of bone cellular communication during one cycle of forced bone remodelling.

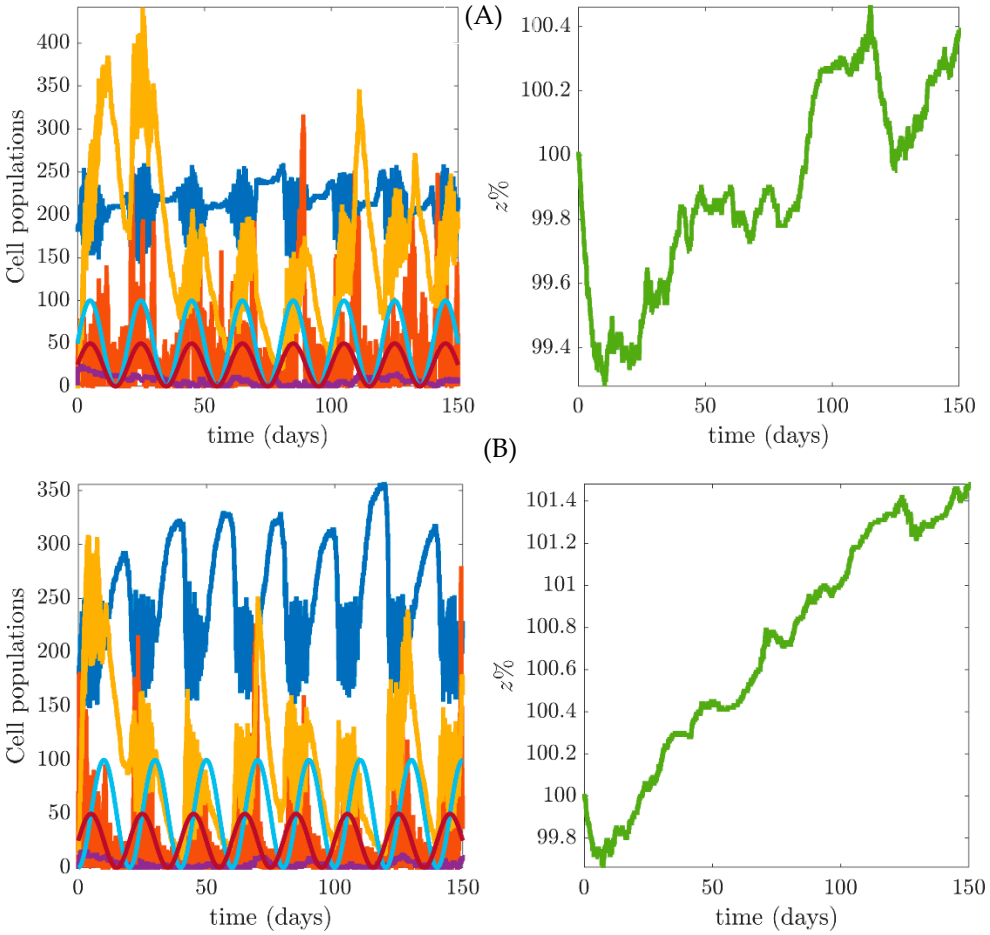

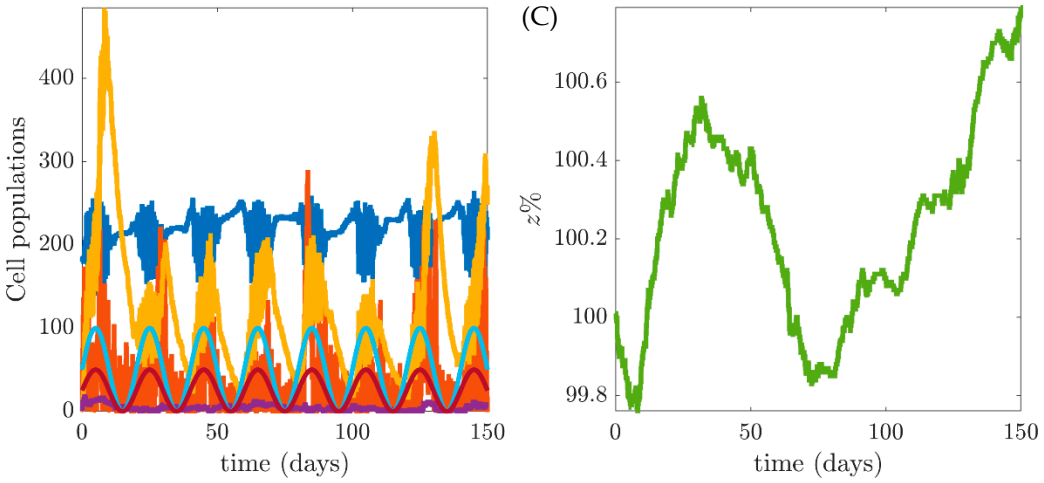


**Figure 8.** External excitation to both the parameter and the source with a reduced source strength $A$. The equations have been altered to ensure that OB does not spike beyond 600, such that the $B$ terms on the right-hand side of all equations are adapted to become $2B$. Previously, to all Figures 2–7, we had a source strength of $A = 50$, multiplied by the sinusoidal wave. In this image the source strength is $A = 10$. (**A**) Oscillatory external excitation in the source and transduced parameter $\gamma_{31}$ with no delay between signals. (**B**) External periodic source (light blue line) and parameter $\gamma_{31}$ (dark red line) out of synchronization by a factor of $\pi/2$. (**C**) Effect of reducing $k_2$ from $k_2 = 0.015445$ taken from [9] to value $k_2 = 0.014$, whilst keeping all other values the same.

## 4. Discussion of Sensitivity

Keeping the same direction and continuing the previous analysis, we are now investigating the sensitivity of the model to the changes in the amplitude of external excitation applied to the osteocyte population in Equation (10), where we represent the additional term of periodic excitation in the following form:

$$A\left(1 + sin\left(\frac{2\pi t}{F} - S\right)\right) \tag{11}$$

where the amplitude $A$ is varied from 10 to 70 in steps of 10, as it is shown in Figure 9, from top to bottom, respectively. Generally, the frequency is $F = 20$ and the offset is $S = 0$; the other parameters are the same as these of the system presented in Figure 8C. In this section, we vary $A$ to illustrate its effect on the output solutions. Having already established stochastic analogue (8a) and (8b) of our deterministic model, we can find regions in the state space of OB-OC for which the model output meets the optimum criterion of their balanced activity. In the state space of interest, it should be represented as a limit cycle or closed loop of number eight shape, indicating doubling of a period. Essentially, the same sensitivity analysis can be performed with an analysis of variance (ANOVA), which is the basis for the quasi Monte Carlo method of system output estimations of the uncertainties of variables [34]. However, the variance-based methods take long processing time with high computational costs for total effects indices [35]; our approach is much more effective and efficient.

In Figure 9, each row represents a different parameter $A$ value and the values are stated on the $y$-axis of the graphs in the first column on the left. The left column illustrates a single simulation of all trajectories. The next four columns show results obtained from 100 simulations. The second column from the left illustrates the evolution $z$ when averaged over the 100 simulations. The bold line is the mean and the error bars represent the results plus, or minus, one standard error. The next three graphs illustrate the phase dynamics of (OCy, OB), (OCy, OC), and (OC, OB), respectively. Specifically, each graph shows a two-dimensional histogram representing all 100 simulations. The colour of the images illustrates the density of the trajectories, namely, if a region is blue, the solution hardly ever achieves these values. However, if a region is green, then the solution often

visits the values in this region. Critically, we note that if there are consistent oscillations (yellow regions), we would expect to see loops appearing in the phase planes (doubling of yellow regions). Equally, multiple 'hot spots' or green patches illustrate that the system can often be found in different states, i.e., the system is not approximately stationary.

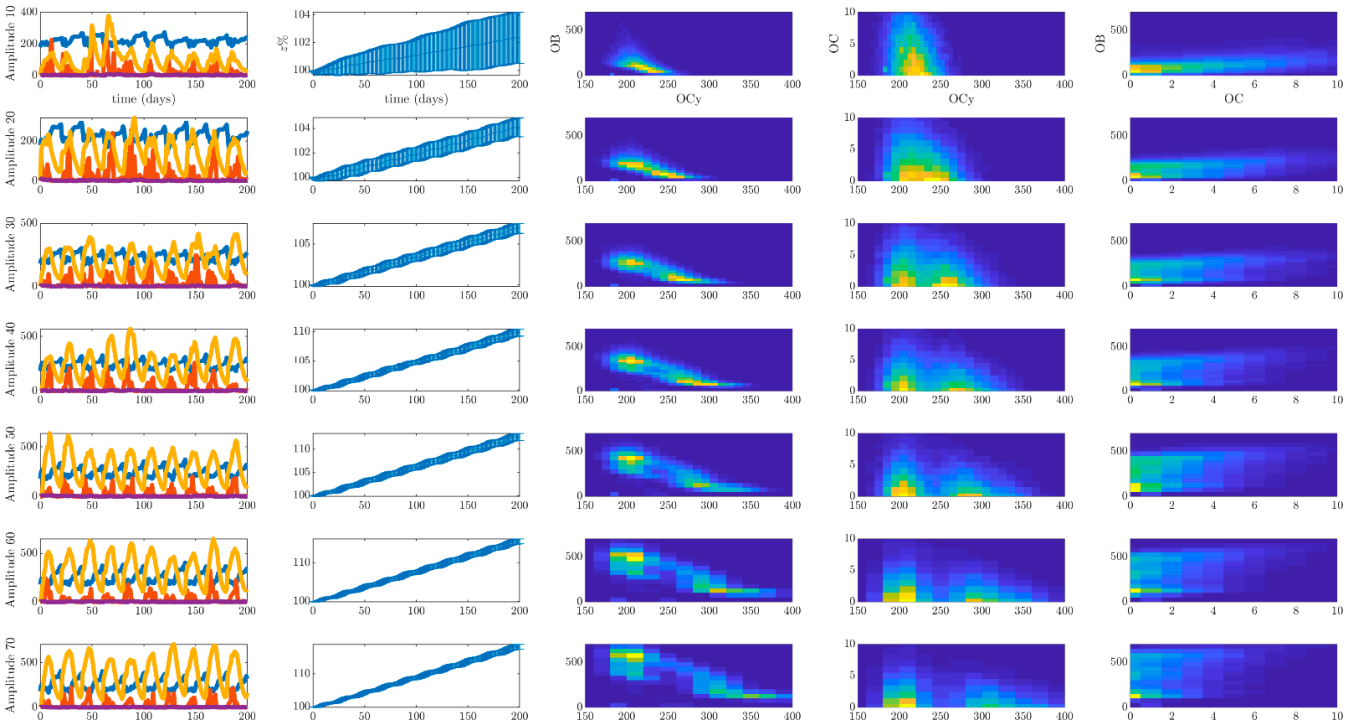


**Figure 9.** A hundred simulations of the stochastic analogue of the bone remodelling model focussing on varying the amplitude parameter of the external loading over the values $A\epsilon\{10, 20, 30, 40, 50, 60, 70\}$.

We observe that increasing $A$ provides three dominant effects. Firstly, it causes $z$ to increase quicker over the 200 days (second column of Figure 9). Secondly, it causes the range of OCy and OB values to increase (third column of Figure 9). Thirdly, it causes the system to become more heavily entrained in the underlying oscillations, as we observe the loop in the third column of Figure 9 becomes larger and clearer. Thus, not all magnitudes of external loading are adequate for regular bone cell lineages activity. For instance, we can find a local bone volume fraction increase beyond 106%, as in Figure 5 from [10], due to the prostate-cancer induced biochemical changes. Such an increase in total bone content in our simulations is present for the amplitude parameter larger than 30.

From the conducted analysis, for example shown in Figure 8, it is clear that the frequency, F, and offset, S, can play a determining role in the deposition of new, remodelled bone tissue. Having established our model of bone cell mechanotransduction, it is possible to find an appropriate set of parameters that satisfy the necessary real conditions of the biological event.

## 5. Conclusions

Osteocytes are recognized as playing a significant role in mechanosensation and transduction of external signals to bone cells, which are engaged in bone remodelling. Mathematical models of bone remodelling have been developed by several authors over the last twenty years [6–9]. Critically, none of the homogenous S-System ODE models account for the presence of external excitation signals. However, the evidence of external signals reception, transduction, delivery, and importance are already experimentally detected and partially clarified. Using the experimental evidence of $Ca^{2+}$ periodical signalling of OcYs [13], we presented a mathematical model of bone mechanobiology, which includes externally periodic forced turnover. Further, we approached the modelling

through both deterministic and stochastic methods, which allow us to consider the intrinsic noisiness of the discrete process.

We discovered that including oscillatory signals with small delays between the received and send signal by OcY provides the closest matches between mathematical theory and biology data. It is straightforward to conclude from Figure 8C where, after the period of resorption (the depression of the green line below the steady-state), we observe a significant activation of osteoblasts that results in a formation period (the green line is above 100%). Comparing the green line in Figure 8C with the green line in Figure 2A (which has no over-formation), we demonstrate that under the influence of the external periodic signal, the local formation of the newly remodelled bone will exceed the amount of resorbed old bone. Furthermore, we investigated the relation between the strength of these two signals and got satisfactory results when the received signal has a smaller value of amplitude. This is our prediction from the model, which must be addressed experimentally. Namely, we require experiments that explore the magnitudes of information that OcY receives and exports. However, we showed that the steady-state value of total bone content changes depending on the external excitation and also on the interplay of other parameter values that influence the dynamics of the process. Using the algebraic computation software package, Maple, we obtained that used steady-state values are the only real steady states within the parameter region of interest. However, it would be interesting and worthwhile to explore the multiple steady states of the presented system with an equation with five ODEs as the base parameters. This will be interesting to discuss in our next in silico research, where we can also investigate the bifurcation regions and the interesting properties of the nonlinear dynamics of the forced S-System. This would give a suggestion for the region of parameters for an applied external signal in a real biological experiment.

**Author Contributions:** Conceptualization of the deterministic model, J.S., and of the stochastic model, T.E.W.; methodology, J.S. and T.E.W.; software calculations, T.E.W.; validation, J.S.; formal analysis, J.S.; investigation, J.S.; resources, J.S. and T.E.W.; data curation, T.E.W.; writing—original draft preparation, J.S.; writing—review and editing, J.S. and T.E.W.; visualization, T.E.W.; supervision, J.S. and T.E.W.; project administration, J.S.; funding acquisition, J.S. All authors have read and agreed to the published version of the manuscript.

**Funding:** A part of this research for the 2020/21 period was financially supported by the Ministry of Education, Science and Technological Development of the Republic of Serbia (Contract No. 451-03-9/2021-14/200109). The results belong in part to the research on project MMoBEER (November 2017–November 2019), funded by the European Union's H2020 MGA MSCA-IF-2016 under grant agreement No. 752793.

**Institutional Review Board Statement:** Not applicable.

**Informed Consent Statement:** Not applicable.

**Data Availability Statement:** All simulations supporting report results can be performed using proposed models.

**Conflicts of Interest:** The authors declare no conflict of interest. The funders had no role in the design of the study; in the collection, analyses, or interpretation of data; in the writing of the manuscript, or in the decision to publish the results.

## References

1. Giorgi, M.; Verbruggen, S.W.; Lacroix, D. In silico bone mechanobiology: Modeling a multifaceted biological system. *Wiley Interdiscip. Rev. Syst. Biol. Med.* **2016**, *8*, 485–505, doi:10.1002/wsbm.1356.
2. Atkins, A.; Milgram, J.; Weiner, S.; Shahar, R. The response of anosteocytic bone to controlled loading. *J. Exp. Biol.* **2015**, *218*, 3559–3569, doi:10.1242/jeb.124073.

3. Xiong, J.; Piemontese, M.; Onal, M.; Campbell, J.; Goellner, J.J.; Dusevich, V.; Bonewald, L.; Manolagas, S.C.; O'Brien, C.A. Osteocytes, not osteoblasts or lining cells, are the main source of the RANKL required for osteoclast formation in remodeling bone. *PLoS ONE* **2015**, *10*, e0138189, doi:10.1371/journal.pone.0138189.
4. Yavropoulou, M.P.; Yovos, J.G. The molecular basis of bone mechanotransduction. *J. Musculoskelet. Neuronal Interact.* **2016**, *16*, 221–236.
5. Bonewald, L.F. Osteocytes: A proposed multifunctional bone cell. *J. Musculoskelet. Neuronal Interact.* 2002, 2(3): 239-241.
6. Komarova, S.V.; Smith, R.J.; Dixon, S.J.; Sims, S.M.; Wahl, L.M. Mathematical model predicts a critical role for osteoclast autocrine regulation in the control of bone remodeling. *Bone* **2003**, *33*, 206–215, doi:10.1016/S8756-3282(03)00157-1.
7. Pivonka, P.; Komarova, S. V Mathematical modeling in bone biology: From intracellular signaling to tissue mechanics. *Bone* **2010**, *47*, 181–189, doi:10.1016/j.bone.2010.04.601.
8. Pivonka, P.; Zimak, J.; Smith, D.W.; Gardiner, B.S.; Dunstan, C.R.; Sims, N.A.; John Martin, T.; Mundy, G.R. Theoretical investigation of the role of the RANK-RANKL-OPG system in bone remodeling. *J. Theor. Biol.* **2010**, *262*, 306–316, doi:10.1016/j.jtbi.2009.09.021.
9. Graham, J.M.; Ayati, B.P.; Holstein, S.A.; Martin, J.A. The Role of Osteocytes in Targeted Bone Remodeling: A Mathematical Model. *PLoS ONE* **2013**, *8*, e63884, doi:10.1371/journal.pone.0063884.
10. Buenzli, P.R.; Pivonka, P.; Gardiner, B.S.; Smith, D.W. Modelling the anabolic response of bone using a cell population model. *J. Theor. Biol.* **2012**, *307*, 42–52, doi:10.1016/j.jtbi.2012.04.019.
11. Matsuo, K.; Irie, N. Osteoclast-osteoblast communication. *Arch. Biochem. Biophys.* **2008**, *473*, 201–209, doi:10.1016/j.abb.2008.03.027.
12. Klein-Nulend, J.; Van Oers, R.F.M.; Bakker, A.D.; Bacabac, R.G. Nitric oxide signaling in mechanical adaptation of bone. *Osteoporos. Int.* **2014**, *25*, 1427–1437, doi:10.1007/s00198-013-2590-4.
13. Morrell, A.E.; Brown, G.N.; Robinson, S.T.; Sattler, R.L.; Baik, A.D.; Zhen, G.; Cao, X.; Bonewald, L.F.; Jin, W.; Kam, L.C.; et al. Mechanically induced Ca2+oscillations in osteocytes release extracellular vesicles and enhance bone formation. *Bone Res.* **2018**, *6*, 1–11, doi:10.1038/s41413-018-0007-x.
14. George, D.; Allena, R.; Rémond, Y. Integrating molecular and cellular kinetics into a coupled continuum mechanobiological stimulus for bone reconstruction. *Contin. Mech. Thermodyn.* **2019**, *31*, 725–740, doi:10.1007/s00161-018-0726-7.
15. Jerez, S.; Chen, B. Stability analysis of a Komarova type model for the interactions of osteoblast and osteoclast cells during bone remodeling. *Math. Biosci.* **2015**, *264*, 29–37, doi:10.1016/j.mbs.2015.03.003.
16. Medsen, H. *Time Series Analysis*; Chapman & Hall, Taylor & Francis Group: Boca Raton, FL, USA; London, UK; New York, NY, USA, 2008; ISBN 142005967X.
17. Buenzli, P.R. Osteocytes as a record of bone formation dynamics: A mathematical model of osteocyte generation in bone matrix. *J. Theor. Biol.* **2015**, *364*, 418–427, doi:10.1016/j.jtbi.2014.09.028.
18. Simonović, J. Simultaneous Multi-Parametric Analysis of Bone Cell Population Model. In *New Trends in Nonlinear Dynamics*; Lacarbonara, W., Balachandran, B., Ma, J., Tenreiro Machado, J.A., Stepan, G., Eds.; Springer International Publishing: Cham, Switzerland, 2020; pp. 233–241, ISBN 978-3-030-34723-9.
19. Giorgio, I.; dell'Isola, F.; Andreaus, U.; Alzahrani, F.; Hayat, T.; Lekszycki, T. On mechanically driven biological stimulus for bone remodeling as a diffusive phenomenon. *Biomech. Modeling Mechanobiol.* **2019**, *18*, 1639–1663.
20. Woolley, T.E.; Baker, R.E.; Gaffney, E.A.; Maini, P.K. Stochastic reaction and diffusion on growing domains: Understanding the breakdown of robust pattern formation. *Phys. Rev. E Stat. Nonlinear Soft Matter Phys.* **2011**, *84*, 046216, doi:10.1103/PhysRevE.84.046216.
21. Savageau, M.A.; Voit, E.O. Recasting nonlinear differential equations as S-systems: A canonical nonlinear form. *Math. Biosci.* **1987**, *87*, 83–115, doi:10.1016/0025-5564(87)90035-6.
22. Kampen, V.N.G. *Stochastic Processes in Physics and Chemistry*; Elsevier: Amsterdam, The Netherlands, 2007; ISBN 9780444529657.
23. Gillespie, D.T. Stochastic Simulation of Chemical Kinetics. *Annu. Rev. Phys. Chem.* **2007**, 58, 35–55, doi:10.1146/annurev.physchem.58.032806.104637.
24. Gillespie, D.T. A general method for numerically simulating the stochastic time evolution of coupled chemical reactions. *J. Comput. Phys.* **1976**, *22*, 403–434, doi:10.1016/0021-9991(76)90041-3.
25. Schumacher, L.J.; Woolley, T.E.; Baker, R.E. Noise-induced temporal dynamics in Turing systems. *Phys. Rev. E Stat. Nonlinear Soft Matter Phys.* **2013**, *87*, 042719, doi:10.1103/PhysRevE.87.042719.
26. Belmonte-Beitia, J.; Woolley, T.E.; Scott, J.G.; Maini, P.K.; Gaffney, E.A. Modelling biological invasions: Individual to population scales at interfaces. *J. Theor. Biol.* **2013**, *334*, 1–12, doi:10.1016/j.jtbi.2013.05.033.
27. Woolley, T.E.; Baker, R.E.; Gaffney, E.A.; Maini, P.K. Power spectra methods for a stochastic description of diffusion on deterministically growing domains. *Phys. Rev. E Stat. Nonlinear Soft Matter Phys.* **2011**, *84*, 021915, doi:10.1103/PhysRevE.84.021915.
28. Woolley, T.E.; Baker, R.E.; Gaffney, E.A.; Maini, P.K. Influence of stochastic domain growth on pattern nucleation for diffusive systems with internal noise. *Phys. Rev. E Stat. Nonlinear Soft Matter Phys.* **2011**, *84*, 041905, doi:10.1103/PhysRevE.84.041905.
29. Murray, J.D. *Mathematical Biology I. An Introduction*, 3rd ed.; Springer: New York, NY, USA; Berlin/Heidelberg, Germany, 2002; Volume 1; ISBN 0387952233.
30. Zumsande, M.; Stiefs, D.; Siegmund, S.; Gross, T. General Analysis of Mathematical Models for Bone Remodeling. *Bone* **2011**, *48*, 910–917, doi:10.1016/j.bone.2010.12.010.

31. Chou, I.C.; Voit, E.O. Recent developments in parameter estimation and structure identification of biochemical and genomic systems. *Math. Biosci.* **2009**, *219*, 57–83, doi:10.1016/J.MBS.2009.03.002.
32. Nobile, M.S.; Tangherloni, A.; Rundo, L.; Spolaor, S.; Besozzi, D.; Mauri, G.; Cazzaniga, P. Computational Intelligence for Parameter Estimation of Biochemical Systems. In Proceedings of the 2018 IEEE Congress on Evolutionary Computation (CEC), Rio de Janeiro, Brazil, 8–13 July 2018; pp. 1–8, doi:10.1109/CEC.2018.8477873.
33. Maplesoft, Inc. *A Division of Waterloo Maple 2019*; Maplesoft, Inc.: Waterloo, ON, Canada, 2019.
34. Sobol, I.M. Global sensitivity indices for nonlinear mathematical models and their Monte Carlo estimates. *Math. Comput. Simul.* **2001**, *55*, 271–280, doi:10.1016/S0378-4754(00)00270-6.
35. Saltelli, A.; Annoni, P.; Azzini, I.; Campolongo, F.; Ratto, M.; Tarantola, S. Variance based sensitivity analysis of model output. Design and estimator for the total sensitivity index. *Comput. Phys. Commun.* **2010**, *181*, 259–270.